Cell

The Postsynaptic Density Proteins Homer and Shank Form a Polymeric Network Structure

Mariko Kato Hayashi,[1,2,*] Chunyan Tang,[3] Chiara Verpelli,[4] Radhakrishnan Narayanan,[1] Marissa H. Stearns,[1,6] Rui-Ming Xu,[5,7] Huilin Li,[3] Carlo Sala,[4] and Yasunori Hayashi[1,2]

[1]RIKEN-MIT Neuroscience Research Center, The Picower Institute for Learning and Memory, Department of Brain and Cognitive Sciences, Massachusetts Institute of Technology, Cambridge, MA 02139, USA

[2]Brain Science Institute, RIKEN, Wako, Saitama 351-0198, Japan

[3]Biology Department, Brookhaven National Laboratory, Upton, NY 11973, USA

[4]Consiglio Nazionale delle Ricerche, Institute of Neuroscience and Department of Pharmacology, University of Milan, 20129 Milan, Italy

[5]Structural Biology Program, The Helen L. and Martin S. Kimmel Center for Biology and Medicine at the Skirball Institute of Biomolecular Medicine and Department of Pharmacology, New York University School of Medicine, New York, NY 10016, USA

[6]Present address: Graduate Program in Neuroscience, Department of Biology, Brandeis University, Waltham, MA 02453, USA

[7]Present address: Institute of Biophysics, Chinese Academy of Sciences, 15 Da Tun Road, Beijing 100101, China

*Correspondence: hayashim@mit.edu

DOI 10.1016/j.cell.2009.01.050

SUMMARY

The postsynaptic density (PSD) is crucial for synaptic functions, but the molecular architecture retaining its structure and components remains elusive. Homer and Shank are among the most abundant scaffolding proteins in the PSD, working synergistically for maturation of dendritic spines. Here, we demonstrate that Homer and Shank, together, form a mesh-like matrix structure. Crystallographic analysis of this region revealed a pair of parallel dimeric coiled coils intercalated in a tail-to-tail fashion to form a tetramer, giving rise to the unique configuration of a pair of N-terminal EVH1 domains at each end of the coiled coil. In neurons, the tetramerization is required for structural integrity of the dendritic spines and recruitment of proteins to synapses. We propose that the Homer-Shank complex serves as a structural framework and as an assembly platform for other PSD proteins.

INTRODUCTION

The postsynaptic density (PSD) is an electron-dense structure attached to the cytoplasmic surface of the excitatory postsynaptic membrane in the central nervous system. It is considered to play a major role in the function and structure of the synapse (Okabe, 2007; Sheng and Hoogenraad, 2007). The PSD consists of hundreds of proteins, which are involved in diverse functions such as signal transduction, structural regulation, and metabolism. In contrast to our extensive knowledge of the constituents of the PSD, the molecular architecture that retains the structure of the PSD is not fully understood.

Homer/cupidin/Vesl/PSD-Zip45 and Shank/ProSAP/Spank/CortBP/Synamon/SSTRIP are among the most abundant scaffolding proteins in the PSD. Homer is alternatively spliced into long and short forms (Figure 1A). The long forms contain an EVH1 (Ena/VASP homology 1) domain and a coiled-coil region, which forms a homotetramer (Hayashi et al., 2006). In contrast, the short forms are monomers containing only the EVH1 domain. The EVH1 domain binds to various scaffolding and signal transduction molecules, such as type I metabotropic glutamate receptors (mGluR), IP_3 receptors (IP_3R), Shank, transient receptor potential canonical (TRPC) family channels, and dynamin3 (Shiraishi-Yamaguchi and Furuichi, 2007; Worley et al., 2007). The crystal structure of the Homer EVH1 domain was solved, showing the mechanism of mGluR binding (Beneken et al., 2000). On the other hand, the three-dimensional structure of the coiled-coil region and hence the overall structure of Homer is unknown.

Shank is among the most abundant binding partners of Homer in the PSD (Cheng et al., 2006). It has an N-terminal ankyrin repeat domain, an SH3 (Src homology 3) domain, a PDZ (PSD-95/Discs large/zona occludens-1) domain, a long proline-rich sequence containing binding sites for Homer and cortactin, and a C-terminal SAM (sterile alpha motif) domain (Figure 1A) (Naisbitt et al., 1999; Tu et al., 1999). Through these domains, Shank interacts with many signaling and scaffolding molecules. Homer and Shank are major determinants of the size of dendritic spines and the PSD. Overexpression of Shank in neurons results in enlargement of dendritic spines, and the effect is significantly enhanced by coexpression of the long form of Homer (Sala et al., 2001).

In this study, we found that Homer and Shank form a high-order-polymerized complex with a mesh-like network structure. This complex recruited another postsynaptic protein, GKAP/SAPAP/DAP-1, which serves as an interface between Shank and PSD-95. The subsequent X-ray crystallographic analysis of the coiled-coil region revealed a characteristic antiparallel tetrameric arrangement. This tetrameric structure is critical for forming the high-order complex, which in turn is necessary for the structural and functional integrity of dendritic spines. We propose that this Homer-Shank complex is the structural framework of the PSD, which serves as a binding platform for other synaptic proteins.

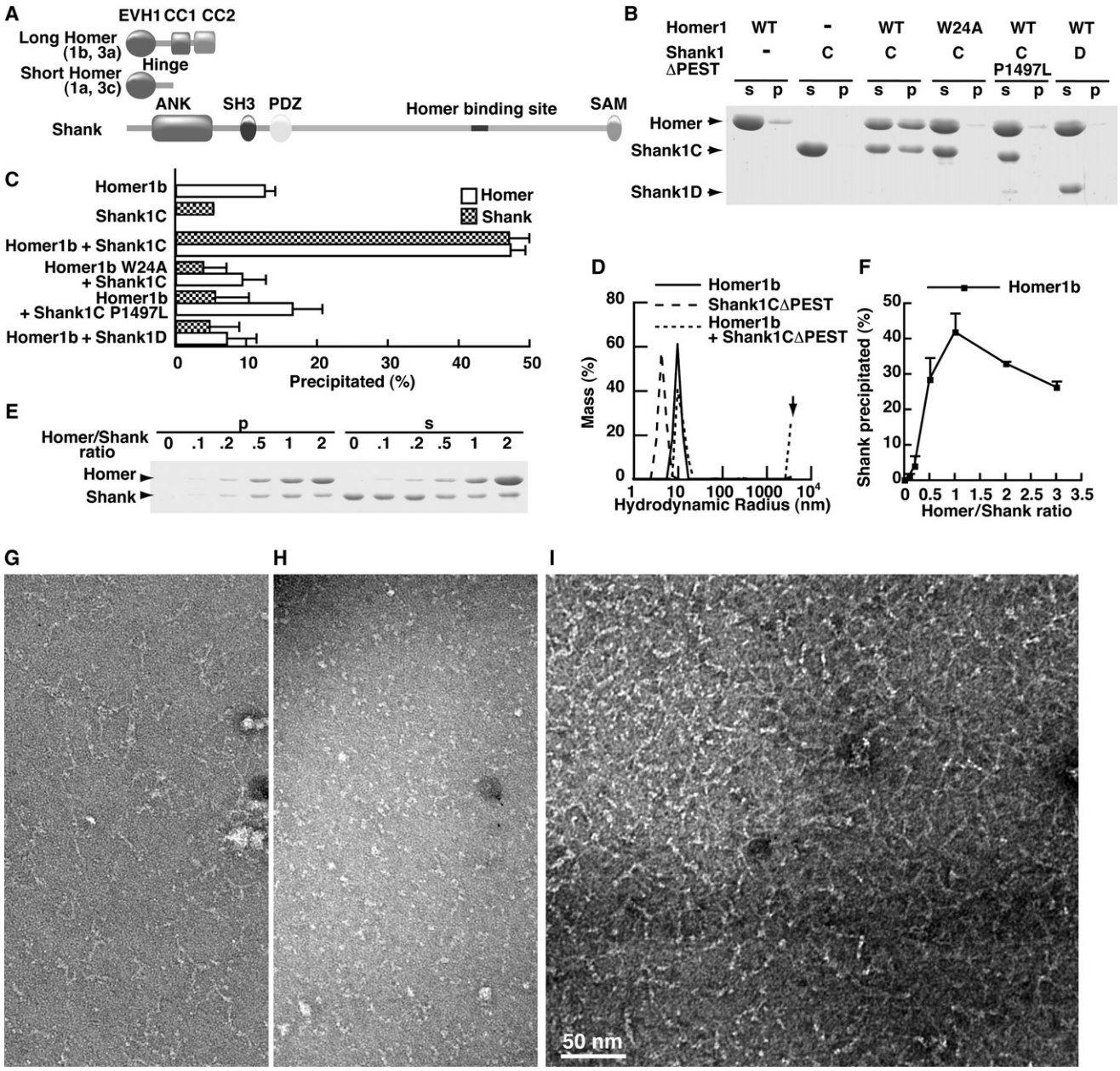

Figure 1. Formation of a High-Order Complex between Homer and Shank

(A) Domain structures of Homer and Shank.

(B) Formation of a high-order complex between Homer1b and Shank1CΔPEST. Homer and Shank were mixed at a concentration of 19 μM each and centrifuged after overnight incubation at 4°C. The pellets (p) and the supernatants (s) in the same volume were separated by SDS-PAGE and stained by Coomassie. Shank1CΔPEST ("C") is a construct with the PDZ domain, the Homer binding site, and a SAM domain. Shank1DΔPEST ("D") is a construct with the PDZ domain and the Homer binding site.

(C) A summary of four repeated experiments similar to (B). Error bars show standard errors.

(D) Hydrodynamic radius distribution measured by dynamic light scattering of Shank, Homer, and a mixture of the two. The arrow indicates a high-order complex. Note that because this peak is at the upper limit of measurement, at 3.6 μm, the reading of mass (%) estimated as globular proteins could be inaccurate.

(E) The stoichiometry of the complex between Homer1b and ShankC1ΔPEST. Increasing concentrations (0–19 μM) of Homer1b were added to a fixed concentration of Shank (9.6 μM).

(F) The summary of the amount of Shank precipitate in three repeated experiments similar to (E).

(G–I) Electron microscopy images of Homer, Shank, and Homer-Shank complex. Negative stain images of Homer1b (0.4 μM) (G), Shank1CΔPEST (0.4 μM) (H), and complex formed in the 1:1 molar ratio mixture of Homer1b and Shank1CΔPEST, each at 1 μM (I).

RESULTS

Formation of a High-Order Complex between Homer and Shank

Overexpression of Shank in neurons causes enlargement of dendritic spines, and coexpression of a long Homer, Homer1b, with Shank synergistically enhances the effect (Sala et al., 2001). We were intrigued by how Shank causes the enlargement of dendritic spines with a synergistic effect of Homer. Shank is known to homomultimerize through interactions between its domains (Baron et al., 2006; Im et al., 2003; Romorini et al., 2004), while Homer1b forms a tetramer (Hayashi et al., 2006). We hypothesized that the tetrameric Homer crosslinks the multimeric Shank, resulting in the formation of a polymerized matrix structure. Such a complex does not have any theoretical limit in size and reasonably explains the synergistic effect of Homer and Shank on the size of dendritic spines.

To test this hypothesis, we attempted to reconstitute the high-order complex using purified Shank and Homer1b. For stable expression and purification of Shank, we deleted the ankyrin repeats, the SH3 domain, and the proline-rich region predicted to be PEST sequences while leaving the Homer binding site intact. This deletion construct retains the PDZ domain, the Homer binding site, and the SAM domain and was named Shank1CΔPEST, based on a naturally occurring alternatively spliced form of Shank1 lacking the N-terminal domains (Lim et al., 1999).

The high-order complex formation was assessed by high-speed centrifugation. When tested individually, neither the purified Shank1CΔPEST nor Homer1b formed precipitate upon ultracentrifugation (Figures 1B and 1C). In contrast, when they were mixed at a 1:1 molar ratio, approximately 50% of Shank1CΔPEST and Homer1b were precipitated, suggesting the formation of a high molecular weight complex. On dynamic light scattering, a sensitive method for detecting large complex, Homer1b or Shank1CΔPEST alone had a single scattering peak corresponding to the hydrodynamic radii of 10.3 and 4.3 nm, respectively (Figure 1D). In contrast, the mixture of Homer1b and Shank1CΔPEST showed two peaks, one at 12.1 nm and the other at 3.6 μm, the upper limit of our instrument (Figure 1D). The latter peak corresponds to the polymerized complex between Homer1b and Shank1CΔPEST. The first peak, slightly larger than Homer1b alone, shows the interaction between Homer1b and Shank1CΔPEST.

Formation of the high-order complex required the specific interaction between Homer1b and Shank. Neither a Homer1b W24A mutant without the EVH1 domain ligand-binding activity (Beneken et al., 2000) nor Shank1CΔPEST P1497L mutant with a mutation at the Homer binding site (Lim et al., 1999) formed the precipitate (Figures 1B and 1C). Shank1CΔPEST without the SAM domain (Shank1DΔPEST) did not form precipitates with Homer1b either, indicating that multimerization of Shank is required for the high-order complex formation. When varying amounts of Homer1b were incubated with a fixed amount of Shank1CΔPEST, the amount of Shank1CΔPEST in the precipitate was maximum when Homer and Shank were at a 1:1 ratio (Figures 1E and 1F).

The formation of the high-order matrix structure was further confirmed by negative stain electron microscopy. When observed individually, Homer1b appeared as highly flexible fibers, which likely represent the coiled-coil domain (Figure 1G). Shank1CΔPEST had a globular structure, which likely represents the oligomerized SAM domains and the PDZ domains (Figure 1H). In contrast, the Homer and Shank mixture showed a mesh-like structure in electron microscopic images (Figure 1I). The mesh appears to contain hubs, possibly representing Shank oligomerized via its SAM domain and linked by the filamentous Homer.

Interaction between Homer-Shank High-Order Complex and Other Synaptic Proteins

The mesh-like structure observed under electron microscopy is consistent with its ability to incorporate other PSD proteins. We therefore wanted to know if the Homer-Shank complex can recruit other PSD proteins. GKAP, another abundant PSD protein, was chosen for its ability to bind to Shank and PSD-95 (Naisbitt et al., 1999; Tu et al., 1999). When purified C-terminal fragment of GKAP (451–666) was incubated with Homer and Shank, the GKAP fragment coprecipitated with the Homer-Shank complex without affecting the amount of Homer or Shank in the precipitates (Figures 2A and 2B). The amount of GKAP in the precipitates reached the plateau at the molar ratio of ~1.4 versus Homer/Shank.

We also examined whether the Homer1b and Shank complex formation can be regulated by mechanisms related to synaptic plasticity. First, we observed the effect of Homer1a, an activity-induced form of Homer (Figure 1A). We added increasing amounts of Homer1a to a fixed amount of Homer1b-Shank1CΔPEST mixture. Precipitation was decreased to half when Homer1a was added at a ratio of 1:1 and fully prevented at a 5-fold excess of Homer1a to Homer1b (Figures 2C and 2D). This indicates that a competitive interaction between Homer1a and Homer1b on Shank prevents the complex formation.

Ca^{2+}/calmodulin-dependent protein kinase II (CaMKII) is a key regulator of synaptic plasticity. Three CaMKII phosphorylation sites have been identified in Homer3a (Mizutani et al., 2008). We examined the effect of CaMKII-mediated phosphorylation on the formation of a Homer-Shank high-order complex. By adding the purified CaMKIIα activated with Ca^{2+} and calmodulin to the mixture of Homer and Shank (Figures 2E and 2F), the complex formation between Homer3a and Shank1CΔPEST was inhibited, but not the complex formation between Homer1b and Shank1CΔPEST.

The Coiled-Coil Region of Homer Forms a Hybrid of Dimer and Tetramer

The filamentous appearance of Homer, which connects hubs of Shank, suggests the importance of the coiled-coil region of Homer for the Homer-Shank network structure formation. To understand the structural basis of the functional importance of the coiled-coil region, we crystallized the C-terminal 65 residues of Homer1b, which corresponds to one-third of the entire coiled-coil region (Figure 3). The 1.75 Å crystal structure was solved by the multiple-wavelength anomalous dispersion method, using an L308M mutant designed for selenomethionine labeling, and refined to an R/R_{free} of 0.216/0.289 (see Table S1 for statistics). Most of the residues of the crystallized fragments were well ordered, and we could assign most of them to the electron density, with the exception of one or two residues from both termini. The C-terminal 75-residue fragment of Homer3a was

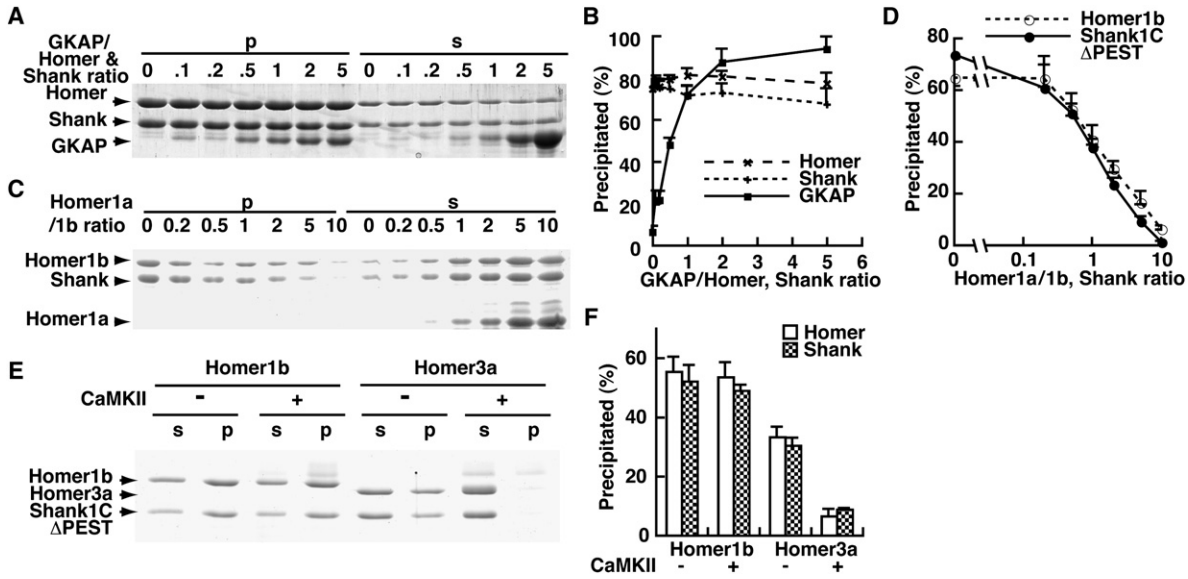

Figure 2. Interaction between the Homer-Shank Complex and Other PSD Proteins

(A) Interaction of GKAP with the high-order complex between Homer and Shank. Increasing concentrations (0–26 μM) of GKAP fragment were added to the fixed amount of Homer1b and Shank1CΔPEST (4.3 μM each) and then centrifuged.

(B) The summary of three independent experiments similar to (A). The fraction of Homer1b and Shank1CΔPEST in the precipitate and the amount of GKAP in the precipitate expressed with the intensity of precipitated Homer1b as 100% were plotted.

(C and D) Dose-dependent inhibition of the high-order complex formation between Homer and Shank by Homer1a. Increasing concentrations (0–190 μM) of Homer1a were added to Homer1b and Shank1CΔPEST (19 μM each) and centrifuged. (D) shows the summary of four repeated experiments.

(E and F) Effect of CaMKII phosphorylation on the high-order complex formation between Homer and Shank. CaMKIIα activated by calcium and calmodulin were added to Homer1b or Homer3a and Shank1CΔPEST (8 μM each), then centrifuged after 30 min incubation at 25°C. (F) shows the summary of three repeated experiments.

also crystallized, and the 2.9 Å structure was solved by the molecular replacement method, using the Homer1b structure as a search model, and refined to an R/R_{free} of 0.252/0.287. The root mean square deviations of Cα positions between each strand of the two structures were 0.72–1.09 Å. Due to the high structural similarity between Homer3a and Homer1b, we use Homer1b for analyses and discussions in the remainder of this study.

The structure showed an elongated rod-like structure 140 Å in length (Figure 3A). It consists of two pairs of parallel left-handed dimeric coiled coils intercalating with each other at the very C termini, where it forms an antiparallel tetrameric coiled coil. The diameter of the coiled coil at the dimeric region of each end is 15 Å, and the diameter at the tetrameric region at the center is 25 Å.

The overall length of the coiled-coil region is ~180 residues, which can be translated to ~45 nm. Upstream of the coiled-coil region, there is a hinge region of ~60 residues and the N-terminal globular EVH1 domain. As a whole, Homer has a dumbbell-like tetrameric structure with a pair of EVH1 domains located at each end of the tetramer, separated by a dimer-tetramer hybrid coiled coil (Figure 3B).

The primary sequence of the N-terminal portion of the dimeric region (290–312) shows typical heptad repeats with the *a* and *d* positions occupied by aliphatic or small polar amino acids (Figures 3C and 3E). Most of the residues at the *a* and *d* positions form canonical knobs-into-holes interactions. The *e* and *g* positions are occupied by acidic or basic residues and are involved in the formation of intermolecular salt bridges (Figures 3E and 3F).

The space between the two helices starts to widen around residue 312 toward the carboxyl side, thus allowing accommodation of larger amino acids at *a* and *d* positions such as Q319 (*a* position) and F322 (*d* position) (Figures 3D, 3E, and 3G). Knobs-into-holes packing is rarely observed within this region. Eventually, the distance becomes sufficiently wide for the intercalation of another dimer to form a tail-to-tail tetramer in a left-handed antiparallel configuration via the C-terminal 30 residues (Figures 3A, 3D, and 3E). In the tetrameric region (326–354), the *e* positions, in addition to the *a* and *d* positions, are occupied by hydrophobic residues, typically leucine and isoleucine (Figures 3C and 3E). Unlike the dimeric region, the knobs-into-holes interactions are observed between the residues at the *d* (A-D and B-C) and *e* (A-C and B-D) positions (Figure 3H). The residues at the *a* positions, all occupied by leucines, do not form knobs-into-holes interactions but fill the cavity at the center of the four α helices, thereby forming a hydrophobic core (Figure 3I). No fixed water molecules were observed in this cavity.

A Dimeric Mutant of Homer1b Does Not Form a High-Order Complex with Shank

To explore the functional significance of the unusual antiparallel tetrameric structure, we attempted to disrupt this structure and dimerize by introducing point mutations based on the crystal structure. In the dimeric coiled-coil region, positively or negatively charged residues at the *e* and the *g* positions are common, and they form either inter- or intrachain salt bridges to stabilize the dimer, while these positions are occupied by aliphatic residues

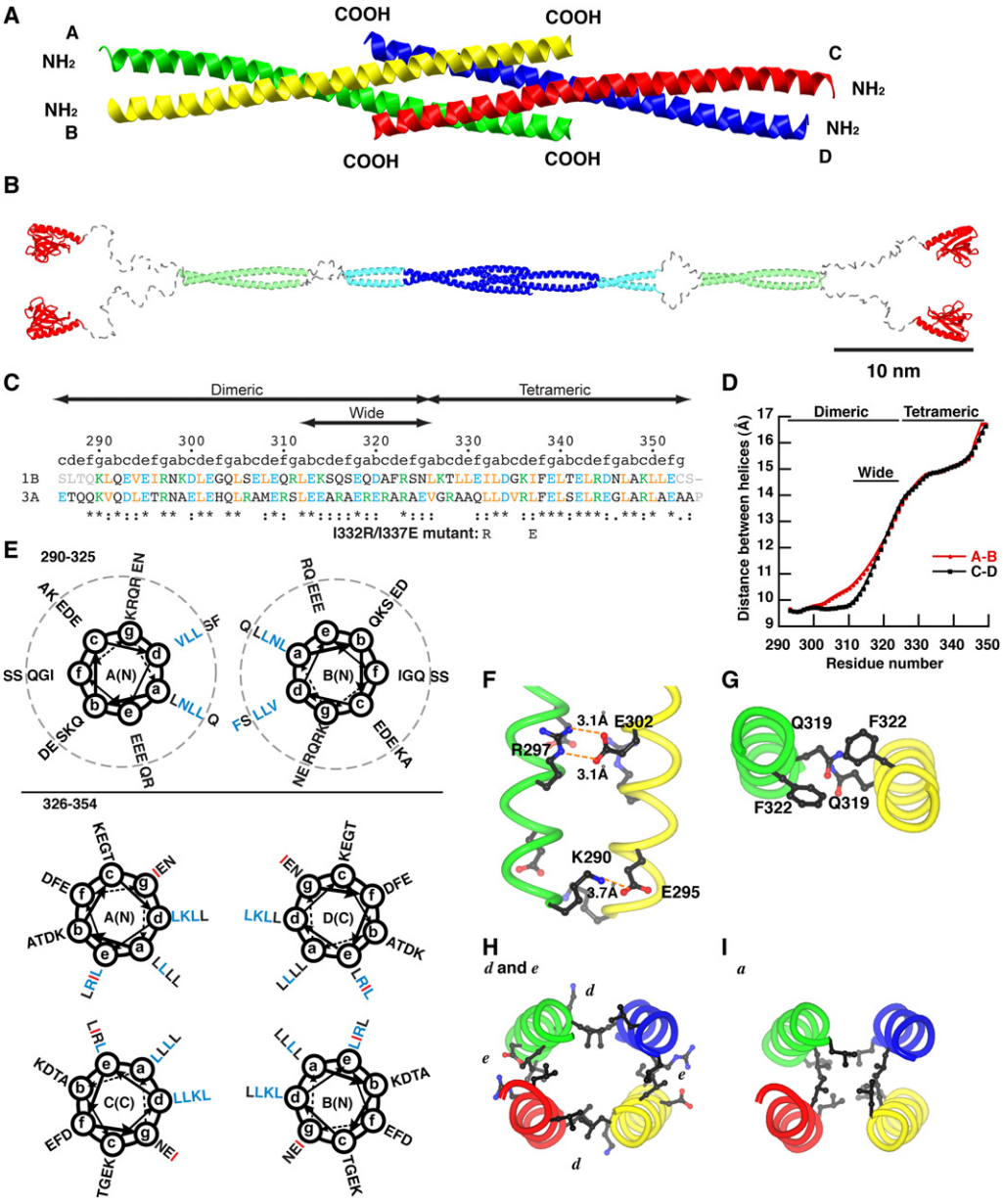

Figure 3. Crystal Structure of the Homer Coiled-Coil Region

(A) Ribbon representation of the crystal structure of the C-terminal half of Homer1b coiled-coil region CC2. The four strands are marked A–D.

(B) A model of the whole structure of long form of Homer. The model is constructed from the structure of the Homer1CC2 domain (blue), EVH1 domain (red) (Irie et al., 2002), and coiled-coil probability prediction and protease degradation sites (Hayashi et al., 2006). The CC1 and a part of the CC2 domain, whose atomic structures are not known, are in light green and light blue, respectively. Regions likely to be disordered are shown in gray.

(C) Primary sequence of the crystallized fragment. 1B, rat Homer1b; 3A, human Homer3a. Orange, aliphatic residues (I, L, V); blue, acidic (D, E); green, basic (K, R); gray, residues not in crystals. Mutations made in dimeric Homer1b I332R/I337E are shown below. "abcdefg" denotes positions in the heptad of coiled coil.

(D) Distance between the A and the B strand or between the C and the D strand are measured and plotted against the number of residues.

(E) Helical wheel representation of the dimeric (top) and tetrameric (bottom) region of Homer1b. Residues start from K290 at *g* position. Residues that make knobs-into-holes interactions with residues on the other strands are shown in blue. Residues changed in the dimeric mutant (I332 and I337) are shown in red. Residues outside the dotted circles are located within the wide dimeric region.

(F) Example of intermolecular salt bridges formed between residues at the *e* (E295 and E302) and *g* (K290 and R297) positions within the dimeric region.

(G) Large amino acids occupying the *a* and *d* positions in the wide dimeric region, Q319 and F322.

(H) Interchain interactions in the tetrameric region. Residues at *d* positions (L329, K336, L343, L350) form the A-D and B-C interface, and those at *e* positions (L330, I337, R344, L351) form the A-C and B-D interface.

(I) Hydrophobic core formed by leucines at *a* positions (L326, L333, L340, L347).

in the tetrameric region (Figures 3E, 3F, and 3H). I337 (*e* position) of Homer1 forms a knobs-into-holes interaction with the adjacent chain (Figure 4A). We expected that changing I337 and the corresponding residue at the *g* position, I332, to a pair of positively and negatively charged residues would destabilize the hydrophobic interaction at the core of the tetramer and result in the formation of a stable dimer through electrostatic interactions between the parallel chains. As expected, the I332R/I337E double mutant had a Stokes radius of 6.8 nm, a significant reduction compared to wild-type Homer1b (10.5 nm) and comparable to that of a deletion mutant of the tetrameric region, Homer1bΔ329 (6.5 nm) (Figure 4B). To determine the oligomerization status unambiguously, we measured the molecular weight by sedimentation equilibrium experiments (Figure 4C). While the wild-type had a molecular weight of 179 kDa, corresponding to 4.2-mer, the I332R/I337E mutant was 85 kDa, corresponding to 2.0-mer, and the Δ329 deletion mutant was 84 kDa, corresponding to 2.1-mer.

We tested if wild-type Homer1b and Homer1b I332R/I337E interact with each other. We tagged them with HA and myc epitopes, respectively, and coexpressed in HEK293T cells. The proteins were separated on an analytical gel filtration column, and their elution profiles were monitored by western blotting. Individually expressed HA-Homer1b and myc-Homer1b I332R/I337E were eluted as a single peak at the expected position of tetramer and dimer, respectively. When these two proteins were coexpressed, their elution profiles showed two peaks, at the tetramer and the dimer molecular weights (Figures 4D and 4E). This shows that the dimeric mutant interacts with wild-type Homer to make heteromeric dimers, although some of the heteromers still form tetramers.

Next, we studied if the tetramerization of Homer is important for Shank crosslinking activity. In both a high-speed centrifuge assay and a dynamic light scattering assay, the dimeric mutant Homer1b I332R/I337E did not show the formation of the high-order complex (Figures 4F and 4G). A small shift in the hydrodynamic radius by the addition of Shank1CΔPEST (from 6.8 to 7.5 nm) shows the interaction between the two proteins. This indicates that the specific spatial arrangement of the four EVH1 domains conferred by the coiled-coil domain is important for the Homer-Shank network formation. In contrast, this mutant does not change its interactions with syntaxin 13, which is known to interact with the coiled-coil region of Homer (Figure 4H) (Minakami et al., 2000).

Tetramerization of Homer1b Is Required for Spine Localization of Homer, Shank, and PSD-95

Using the Homer1b I332R/I337E mutant, we studied the role of tetramerization of Homer in neurons. We first compared the synaptic localization between the wild-type Homer1b and the dimeric mutant. We coexpressed the mGFP-tagged Homer or its mutant with cytosolic red fluorescent protein (DsRed2) to normalize volume in CA1 pyramidal neurons of organotypically cultured hippocampal slices. Homer1b accumulated in spines with an average spine/dendrite ratio of 3.09 ± 0.04 (mean ± SEM) (Figures 5A and 5B). In marked contrast, the localization of the dimeric mutant Homer1b I332R/I332E was significantly reduced (1.49 ± 0.02), comparable to monomeric Homer1a (1.50 ± 0.02). These results show that the tetramer formation is critical for synaptic localization of Homer1b.

Given the importance of tetramerization of Homer1b for the formation of the high-order complex with Shank in vitro, we studied if Homer tetramerization is required for spine localization of Shank. We transfected dissociated cultures of hippocampal neurons with myc-Homer1b or its dimeric mutant. Transfected neurons were identified by anti-myc antibody staining, and the distribution of endogenous Shank was detected by an anti-Shank antibody. The expression of Homer1b I332R/I337E clearly reduced the number and the intensity of Shank clusters (Figures 5C–5E).

To study if the expression of the dimeric mutant also affected the spine localization of other PSD proteins, we immunostained PSD-95, another major PSD protein that binds to receptors. The expression of Homer1b I332R/I337E significantly reduced the number of PSD-95 clusters (Figures 5C–5E). These results suggest that the expression of the dimeric mutant of Homer interferes with normal synaptic localization of Shank by preventing the formation of a high-order complex, and also affects the localization of other synaptic proteins, such as PSD-95.

Tetramerization of Homer1b Is Necessary for Maintenance of Dendritic Spine Structure and Synaptic Function

Next, we investigated whether the tetramerization of Homer1b is required for the integrity of dendritic spine structure. We introduced myc-Homer1b or myc-Homer1b I332R/I337E, along with GFP as a volume-filler, into neurons in hippocampal dissociated culture and measured the morphology and density of spines. Compared with neurons expressing Homer1b, those expressing the dimeric Homer1b I332R/I337E had significantly reduced dendritic spine density (Figures 6A and 6B). The remaining spines were significantly longer and slightly thinner, typical of immature spines, though the difference in spine width did not reach statistical significance (Figure 6B). The same experiments using hippocampal organotypic slice culture showed a similar effect of myc-Homer1b I332R/I337E (data not shown). We also tested the effect of siRNA against Homer1 on the dendritic spine structure (Figures 6C and 6D). The siRNA reduced the number of mature spines, which is consistent with the phenotype of Homer1b I332R/I337E overexpression. There were phenotypic differences of the immature spines, that neurons expressing Homer1b I332R/I337E had fewer, longer spines, while those with Homer1 siRNA had increased number of shorter spines. This could be due to the difference in the mechanisms of suppression between these two methods. Importantly, the effect of siRNA was reversed by a rescue construct of Homer1b^R with silent mutations at the siRNA target sequence, but not with a similar rescue construct with dimeric mutation (Homer1b^R I332R/I337E). In addition, while the coexpression of Homer1b with Shank significantly increased the size of Shank clusters compared with Shank alone, as previously reported (Sala et al., 2001), the effect was not observed in the Homer1b I332R/I337E mutant (Figures 6E and 6F).

Finally, to assess the functional significance of Homer tetramerization on synaptic transmission, we analyzed the AMPA-R- and NMDA-R-mediated excitatory postsynaptic current (EPSC) of neurons transfected with Homer1b or Homer1b I332R/I337E (Figures 6G–6J). The expression of Homer1b caused small and

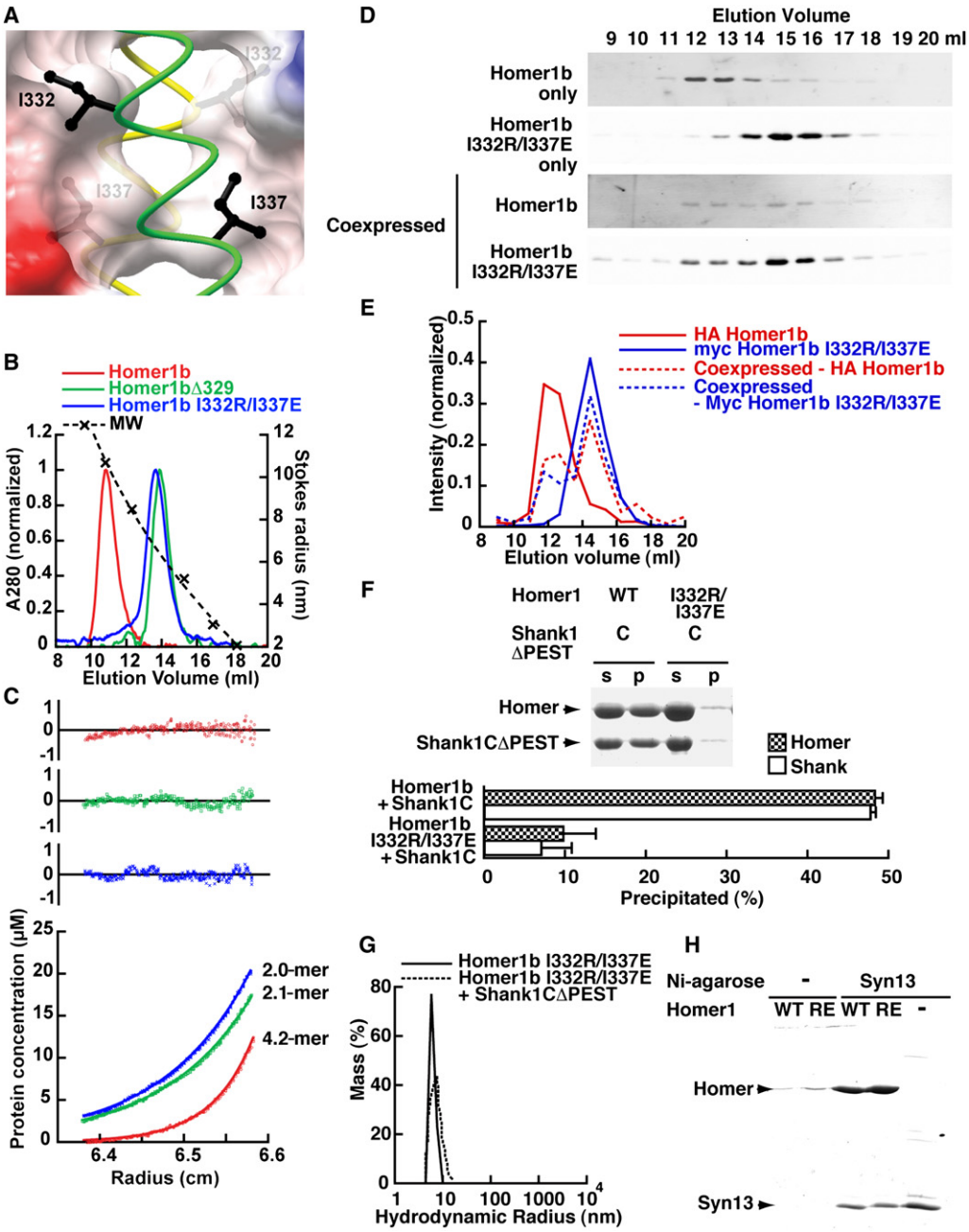

Figure 4. Dimeric Mutants of Homer

(A) Structure around the mutated residues. The A chain (green) and B chain (yellow) are shown with I332 and I337 in black. The surface showing the electrostatic potential of the C and D chains is made half transparent to show the I332 and I337 on strand B.

(B) Elution profiles of purified Homer1b and its mutants from the Superose 6 gel filtration column. The void volume was 8.2 ml.

(C) Representative scans of sedimentation equilibrium analysis of Homer mutants done at centrifuge speed of 12,000 rpm. This sample was also centrifuged at 9,000 rpm and 15,000 rpm and globally fitted to the equilibration model. Deviations from the calculated equilibrium are shown at the top. The same color code as in (B) is used.

(D and E) Disruption of the tetramer of wild-type Homer1b by dimeric Homer1b I332R/I337E mutant. HA-Homer1b and myc-Homer1b I332R/I337E were transfected individually or cotransfected in HEK293T cells. The crude soluble fraction was separated with Superose 6 gel filtration column, and the elution profile of each construct was monitored by western blotting using anti-HA or anti-myc antibody.

(F and G) Loss of Shank crosslinking ability of the dimeric Homer1b I332R/I337E mutant in high-speed centrifugation assay (F) and in dynamic light scattering assay (G). The graph in (F) shows a summary of four repeated experiments.

(H) Intact interaction between syntaxin 13 fragment and Homer1b wild-type or Homer1b I332R/I337E mutant. Crude bacterial lysate expressing Homer1b or Homer1b I332R/I337E was loaded onto Ni-agarose beads with or without hexahistidine-tagged syntaxin 13 fragment and eluted with imidazole. The eluted sample was separated with SDS-PAGE and stained by Coomassie.

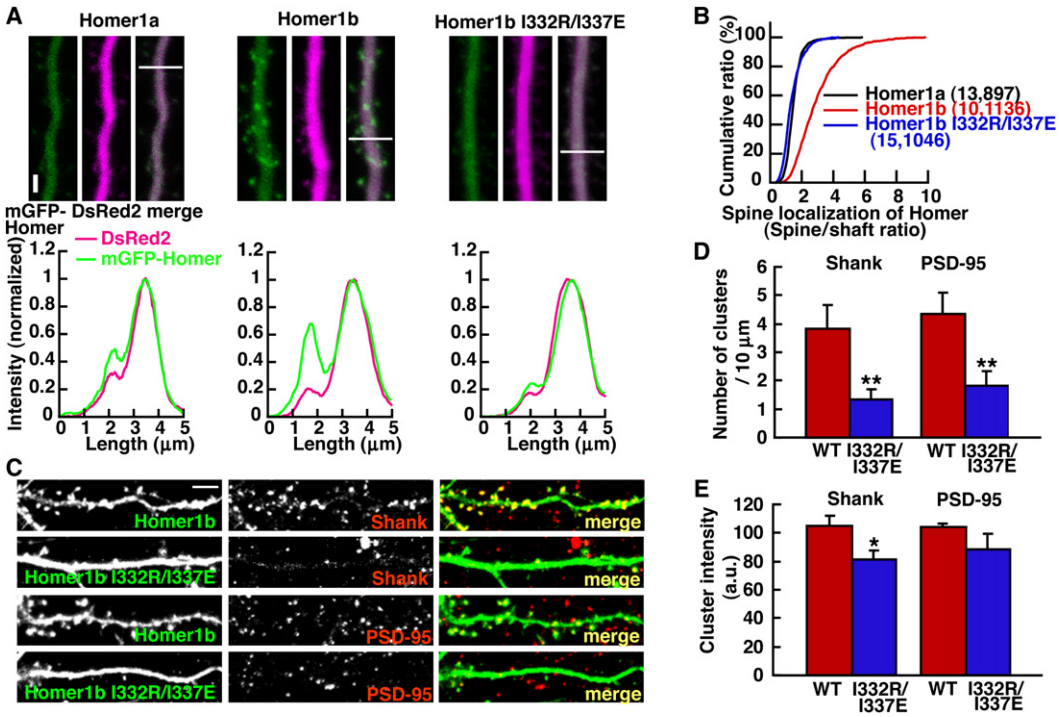

Figure 5. Effect of the Dimeric Mutant Form of Homer on the Localization of Synaptic Proteins

(A) Loss of spine localization of the dimeric mutant of Homer. Representative images of CA1 pyramidal neurons in slice culture transfected with mGFP fusion proteins of Homer1a, Homer1b, Homer1b I332R/I337E (green), and DsRed2 (magenta). The fluorescence profiles across the line in the images are shown at the bottom. The peaks in the middle of the plot correspond with the dendritic shaft, and those to the left are spine heads. The intensity is adjusted so that the peaks in both channels at the dendritic shaft are 1. Scale bar, 2 μm.

(B) Summary of spine localization of different constructs in a cumulative plot. Numbers of cells/spines analyzed are in parentheses.

(C) Representative images of neurons in hippocampal dissociated culture transfected with myc-Homer1b or myc-Homer1b I332R/I337E and stained with anti-myc and anti-Shank or anti-PSD-95. Scale bar, 10 μm.

(D and E) Summary of Shank and PSD-95 cluster density (D) and mean intensity of Shank and PSD-95 clusters (E) (t test: *$p < 0.05$, **$p < 0.01$). Data were obtained from 800–2500 dendritic spines from 6–12 transfected cells.

insignificant increases of both AMPA-R- and NMDA-R-EPSC compared with untransfected neurons (Figures 6H and 6I). On the other hand, expression of Homer1b I332R/I337E caused significant decreases in both currents. The effect is likely due to the combined effect of reduced size and number of dendritic spines and reduced amount of synaptic protein at the synapse. The AMPA/NMDA ratio did not change with the expression of the wild-type or the mutant Homers, suggesting that the effect of the dimerization equally affected the two receptor populations (Figure 6J). These results indicate that tetramerization of Homer1b is important for structure and function of dendritic spines and synapse, through its ability to form a high-order complex with Shank.

DISCUSSION

The Role of Homer and Shank in the PSD Matrix

We found that Homer and Shank form a large precipitable complex, as revealed by biochemistry and electron microscopy (Figures 1 and 7A). Formation of the complex required the tetramerization of Homer, multimerization of Shank, and an interaction between the two proteins. The complex formation was optimal when the molar ratio was close to 1:1. The copy number of Homer and Shank per PSD as monomers is estimated to be anywhere around 60–370 and 150–310, respectively (Cheng et al., 2006; Peng et al., 2004; Sugiyama et al., 2005). Therefore, Shank and Homer exist at an optimal ratio for the formation of a high-order complex. The formation of the Homer-Shank network at around 1:1 stoichiometry reasonably explains the synergistic effect of Shank and Homer on enlargement of spines (Sala et al., 2001).

Further analysis showed that another PSD protein, GKAP, stoichiometrically bound to the complex without disrupting the Homer-Shank complex. GKAP binds to MAGUK proteins such as PSD-95 that further interact with many other synaptic proteins, including AMPA-R and NMDA-R. Related to this in vitro reconstitution, the disruption of endogenous Homer-Shank complex in neurons by dimeric Homer expression reduced the number of immunopositive puncta of both Shank and PSD-95. The same construct also reduced both AMPA-R- and NMDA-R-mediated EPSC. The morphology of dendritic spines was also affected, which could be explained by the fact that Shank also interacts with proteins that physically or functionally associated with the cytoskeleton.

Based on these ultrastructural and biochemical evidences, we propose that the mesh-like complex of Homer and Shank serves as a structural framework for PSD that provides binding platform for other PSD proteins, with a role similar to the gephyrin polymer of inhibitory synapses (Fritschy et al., 2008). The flexible nature of the Homer-Shank matrix may contribute to the dynamic properties of the dendritic spines. Irregular polygonal mesh structure was observed previously in isolated PSD (Petersen et al., 2003). However, we cannot unequivocally conclude the identity of the reported mesh-like structure in native PSD with our reconstituted structure due to the presence of other proteins in the PSD, such as CaMKII, actin, and PSD-95.

There are a few functional differences of the SAM domain between Shank subtypes. The SAM domain of Shank3 was shown by X-ray crystallography and electron microscopy to form helical fibers, and the fibers could be crosslinked by the divalent ion Zn^{2+} into the micrometer-sized sheet structure (Baron et al., 2006). In contrast, Shank1CΔPEST had a molecular weight comparable to a globular protein of 240 kDa, determined by gel filtration analysis (data not shown). The SAM domain is crucial for synaptic localization in Shank3, but not in Shank1 (Boeckers et al., 2005; Sala et al., 2001). Also, Zn^{2+} binds to the SAM domain of Shank3 but not of Shank1 (Baron et al., 2006). The requirement for the SAM domain in the formation of the high-order complex between Homer and Shank seems to conflict with the observation that Shank1 does not require the SAM domain for spine localization or spine enlargement. One explanation is that the interaction between the ankyrin repeats and the SH3 domain of Shank1 can contribute to the multimerization of Shank1 (Romorini et al., 2004) and can theoretically have a similar effect as SAM domain multimerization. We could not test this possibility because the Shank molecule containing the ankyrin repeats and the SH3 domain was not expressed as a soluble protein. Whatever the actual mechanism of Shank multimerization in neurons is, our proposed model of high-order matrix formation between Homer and Shank reasonably explains the observation that the expression level and interaction between these two proteins determines the size of dendritic spines and the PSD (Sala et al., 2001).

Crystal Structure of the Postsynaptic Scaffolding Protein Homer

The crystal structure of the very C terminus of long form of Homer forms an antiparallel tetrameric coiled coil. The entire length of the coiled-coil region is estimated to be approximately 45 nm based on our crystal structure and other known dimeric coiled-coil structures. As a whole, a tetrameric Homer molecule has a dumbbell-like structure with a pair of EVH1 domains at both ends for ligand binding (Figure 3B). The structure may have flexibility at the hinge region and in a region between CC1 and CC2 (Figures 1A and 3B), as these regions appears not to have rigid, ordered structure, as judged by their sensitivity to protease degradation (Hayashi et al., 2006).

This tetrameric arrangement is long enough to span the thickness of the PSD (30–50 nm) or other subcortical cytoskeletal networks. Thus, long form of Homer is capable of connecting a protein on the plasma membrane, such as mGluR or TRPC, with a protein on an intracellular organelle, such as IP_3R, contributing to the functional coupling of these proteins to regulate intracellular Ca^{2+} signaling (Figure 7B). Having two EVH1 domains at each end of the molecule can potentially control the activity of its binding partners through the regulation of their oligomerization or conformational state. For example, mGluR works as a dimer (Kunishima et al., 2000), and TRPC has two Homer binding sites in one subunit and requires binding to both for functional regulation by Homer (Yuan et al., 2003). This configuration also explains how long form of Homer places endocytic zones adjacent to the PSD through interactions with dynamin 3 (Lu et al., 2007).

The spacing of two pairs of EVH1 domains may ensure that each pair of EVH1 domains at both ends interacts with different Shank multimers. Another advantage of being a tetramer is that using one of the four EVH1 domains for interaction with other binding partners will not necessarily interfere with the overall network formation, because the other three EVH1 domains are still available for crosslinking. This enables nondisruptive incorporation of Homer binding proteins to the PSD matrix structure.

We previously suggested that the long form of Homer forms a parallel tetramer based on indirect biophysical and biochemical analyses (Hayashi et al., 2006). Although we correctly concluded that Homer forms a tetramer, we erroneously concluded that it was a parallel tetramer based on a sedimentation equilibrium experiment that showed that the CC1 region of Homer1b forms a tetramer, which led to an assumption that the tetramerization spans the entire coiled-coil region. Our crystallographic analysis of the C-terminal region of the coiled-coil region reported here shows that the two pairs of CC1 regions will be located too far from each other to interact within a tetramer. All other results from our previous study are compatible with the tail-to-tail, dimer-of-dimer model presented in this work. Although CC1 tetramerization does not occur within a tetramer of Homer in the way we initially speculated, it may be involved in interoligomer interactions between Homer tetramers.

Regulation Site for Structural Plasticity of Dendritic Spines

It has been demonstrated that dendritic spines change their shape and size during synaptic plasticity (Hayashi and Majewska, 2005). Given that the Homer-Shank complex is one of the determinants of dendritic spine size, regulation of the stability of the complex may be an underlying mechanism for synaptic plasticity.

One locus for regulating this complex formation is Homer1a. The addition of Homer1a inhibited the formation of the high-order complex in a dose-dependent manner (Figures 2C and 2D). Because the expression of Homer1a is induced by global neuronal activity (Brakeman et al., 1997), this may be one of the mechanisms of homeostatic synaptic plasticity used to reduce the overall activity of a neuron. In fact, overexpression of Homer1a negatively regulates the size of dendritic spines and synaptic transmission (Sala et al., 2003).

Another locus for this regulation is CaMKII phosphorylation. Phosphorylation of Homer3a by CaMKII also inhibited the high-order complex formation between Homer3a and Shank1CΔPEST. Although the inhibition of the high-order complex formation appears to work for weakening of synaptic

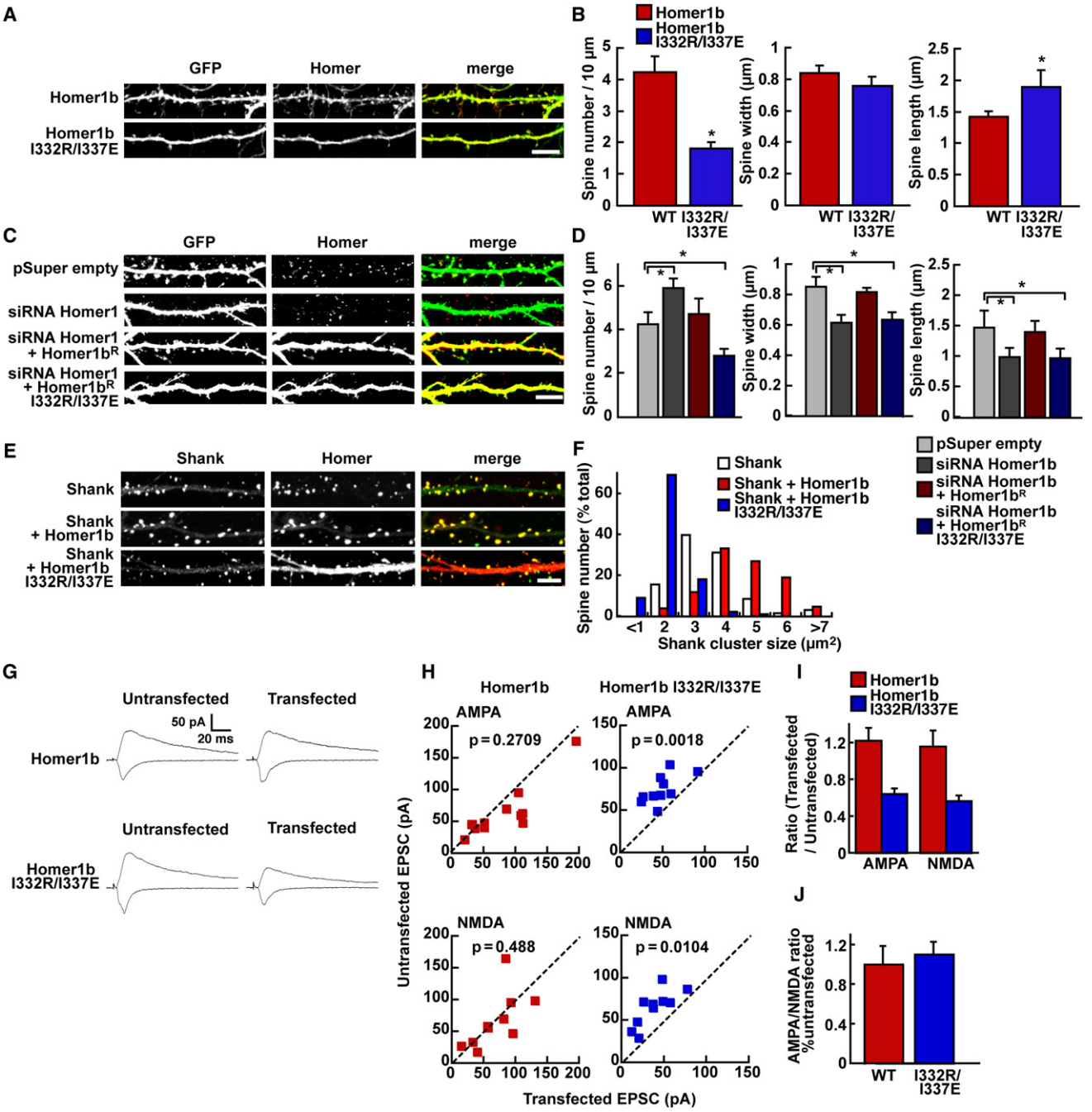

Figure 6. Effect of the Dimeric Mutant Form of Homer on Dendritic Spine Structure and Synaptic Transmission

(A and B) Morphological analysis of dendritic spines expressing Homer1b or Homer1b I332R/I337E using the cytosolic GFP expression. Representative images of hippocampal cultured neurons transfected with myc-Homer1b or myc-Homer1b I332R/I337E and GFP (A) and summary (B). The neurons were stained with anti-myc antibody. *$p < 0.05$ by t test. Data were obtained from 5310 (WT, 8 cells) and 1596 (I332R/I337E, 9 cells) dendritic spines. Scale bar, 10 μm.

(C and D) Morphological analysis of dendritic spines expressing GFP and pSuper empty, GFP and expression vector for siRNA against Homer1b (pSuper-Homer1b); GFP, pSuper-Homer1b, and wild-type Homer1b with mutation that makes it resistant to siRNA (Homer1b^R); or GFP, pSuper-Homer1b and Homer1bR with I332R/I337E mutation (Homer1b^R I332R/I337E). The neurons were stained with anti-Homer1 antibody. (C) Sample images. (D) Data were obtained from 3433 (pSuper empty, 6 cells), 4560 (siRNA Homer1b, 6 cells), 4989 (siRNA Homer1b with Homer1b^R I332R/I337E, 9 cells), and 5633 (siRNA Homer1b with Homer1b^R, 9 cells) dendritic spines. Scale bar, 10 μm.

(E and F) Coexpression of Shank with Homer. The neurons were stained with anti-Shank or anti-Homer1 antibodies. Sample images are shown in (E). Data were obtained from 804 (Shank only, 6 cells), 852 (Shank and Homer1b, 6 cells), and 920 (Shank and Homer1b I332R/I337E, 10 cells) dendritic spines (F). Scale bar, 10 μm.

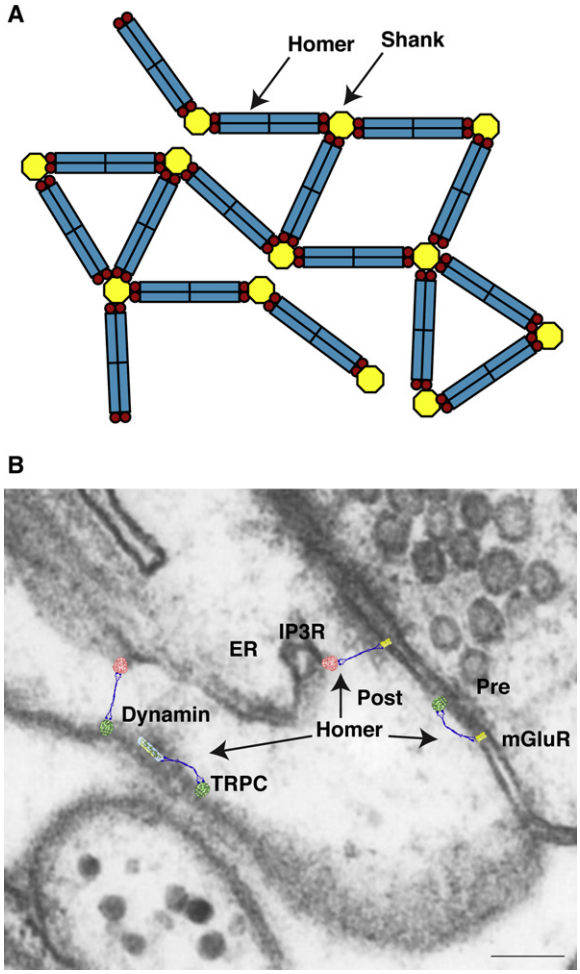

Figure 7. The Model of Interaction between Homer and Shank

(A) A model of high-order complex between Homer and Shank. Currently, the oligomeric status of Shank is not known.

(B) Overlay of the structural model of Homer (blue) on the PSD. The structure of mGluR1 (yellow) is modeled based on the structure of mGluR1 extracellular ligand binding domain (Kunishima et al., 2000) and the structure of rhodopsin (Palczewski et al., 2000). The structures of IP3R (red) (Sato et al., 2004), TRPC (green) (Mio et al., 2007), and dynamin (Mears et al., 2007) are taken from electron microscopy images. All structures are depicted to scale on an electron microscope image of a hippocampal CA1 spine with smooth endoplasmic reticulum, obtained and modified from Spacek and Harris (1997). Copyright 1997 by the Society for Neuroscience. The presynaptic terminal (Pre), postsynaptic terminal (Post), and endoplasmic reticulum (ER) are indicated. Scale bar, 0.1 μm.

transmission, this kind of temporary disassembly of the PSD structure may be required as a process of reorganization of synaptic proteins to form a larger synapse with more efficient synaptic transmission. Activated CaMKII did not affect the high-order complex formation between Homer1b and Shank1CΔPEST, probably due to the lack of a CaMKII phosphorylation site, which affects the complex formation.

Another possible mechanism is the neuronal activity-dependent ubiquitin-proteasome degradation of Shank, mediated by its PEST sequence (Ehlers, 2003; Lee et al., 2008). Such ubiquitination-mediated degradation of Shank will also act to reduce the size of the PSD and spines. These mechanisms may synergistically or nonsynergistically work to disassemble the Homer-Shank complex, leading to the remodeling of the synapse. In these ways, the Homer-Shank high-order complex could be regulated by multiple mechanisms under different aspects of synaptic plasticity.

EXPERIMENTAL PROCEDURES

Crystallization and Data Collection

Rat Homer1CC2 (290–354 [C terminus of Homer1b]) and human Homer3CC2 (287–361 [C terminus of Homer3a]) fragments were purified as described in the Supplemental Data. Purified protein was concentrated with Ultrafree-4 Biomax-10K centrifugal filter concentrators (Millipore; Bedford, MA) to 29 mg/ml (Homer1CC2) or 27 mg/ml (Homer3CC2) for crystallization. Homer1CC2 and Homer3CC2 crystals were grown at 24°C for 2 days by the hanging-drop vapor diffusion method with reservoir solutions of 0.1 M MES, 0.1 M ammonium sulfate, 16% PEG1000, and 10% glycerol (pH 6.0) and 0.1 M Tris, 4.2 M NaCl, and 10% glycerol (pH 7.6), respectively.

The crystals were transferred to the reservoir solution supplemented with glycerol to a final concentration of 20% for cryoprotection and flash-frozen in nitrogen gas stream. Diffraction data were collected using a National Synchrotron Light Source Beamline X26C (Brookhaven National Laboratory; Upton, NY). The methods and statistics of data processing are described in Supplemental Experimental Procedures and Table S1.

High-Speed Centrifugation and Dynamic Light Scattering Assays

For the high-speed centrifugation assay, Shank and Homer were purified as described in the Supplemental Experimental Procedures and mixed at the indicated molar ratio as monomers in buffer with a final concentration of 15 μM in 20 mM potassium phosphate, 0.4 M NaCl, 0.1% 2-mercaptoethanol (pH 7.4) and incubated at 4°C overnight. The samples were centrifuged by Optima TLX Ultracentrifuge (Beckman Coulter; Fullerton, CA) with a TLA-55 rotor at 4°C, 98,560 × *g* for 1 hr. The supernatant and pellet were then recovered. The pellet was resuspended in SDS-PAGE sample buffer at the same dilution as the supernatant and separated using 12% SDS-PAGE gel.

To see the effect of CaMKII phosphorylation, CaMKIIα purified from transfected HEK293-T cells as described in the Supplemental Experimental Procedures and equimolar bovine brain calmodulin (EMD Biosciences; Madison, WI) were incubated in 30 mM HEPES (pH 7.5), 5 mM $MgCl_2$, 0.2 mM $CaCl_2$, 0.1 mM EGTA, and 0.1 mM ATP for 5 min at 25°C. Then, Homer and Shank1CΔPEST were added at the final concentration of 8 μM Homer/8 μM Shank/3 μM calmodulin-CaMKIIα/0.4 M NaCl. The mixture was incubated at 25°C for 30 min, followed by centrifugation as described above.

The measurement of the hydrodynamic radius with dynamic light scattering was carried out at 25°C using the protein mixture prepared as above with DynaPro Titan light scattering system (Wyatt; Santa Barbara, CA). The results shown are representative of more than two independent experiments.

(G and H) Synaptic response from pairs of untransfected control cells and cells transfected with either Homer1b or Homer1b I332R/I337E. Sample traces are shown in (G). Stimulation artifacts are truncated. For each pair of cells, the amplitude of AMPA-R or NMDA-R EPSCs from transfected cell is plotted against that of control cell (H). Homer1b, AMPA-R, n = 11; NMDAR n = 10; AMPA-R/NMDA-R ratio n = 10. Homer1b I332R/I337E, n = 10 for each measurement.

(I) The ratio of amplitude in transfected cells/untransfected cells.

(J) The AMPA-R/NMDA-R-EPSC ratio normalized to the untransfected cells.

SUPPLEMENTAL DATA

Supplemental Data include Supplemental Experimental Procedures, Supplemental References, and one table and can be found online at http://www.cell.com/cell/supplemental/S0092-8674(09)00135-4.

ACKNOWLEDGMENTS

The crystallographic data were deposited in PDB with accession number 3CVE (Homer1b) and 3CVF (Homer3a). We thank Doctors Amy E. Keating, Robert T. Sauer, Myung Jong Kim, Amanda Mower, Teiichi Furuichi, and Morgan Sheng for helpful discussion and sharing of resources, as well as Ms. Cristina Zucchi and Ms. Valentina Giannini for technical help. The Biophysical Instrumentation Facility for the Study of Complex Macromolecular Systems (supported by NSF-0070319 and NIH GM68762) at Massachusetts Institute of Technology is gratefully acknowledged. This work was supported by RIKEN; NIH grant R01DA17310; Grant-in-Aid from the Ministry of Education, Science, and Culture of Japan (Y.H.); Telethon Italy (grant number GGP06208); Fondazione Cariplo (project number 2006-0779/109251); and Compagnia di San Paolo (project number 2005-1964) (C.S.).

Received: April 28, 2008
Revised: November 7, 2008
Accepted: January 23, 2009
Published: April 2, 2009

REFERENCES

Baron, M.K., Boeckers, T.M., Vaida, B., Faham, S., Gingery, M., Sawaya, M.R., Salyer, D., Gundelfinger, E.D., and Bowie, J.U. (2006). An architectural framework that may lie at the core of the postsynaptic density. Science *311*, 531–535.

Beneken, J., Tu, J.C., Xiao, B., Nuriya, M., Yuan, J.P., Worley, P.F., and Leahy, D.J. (2000). Structure of the Homer EVH1 domain-peptide complex reveals a new twist in polyproline recognition. Neuron *26*, 143–154.

Boeckers, T.M., Liedtke, T., Spilker, C., Dresbach, T., Bockmann, J., Kreutz, M.R., and Gundelfinger, E.D. (2005). C-terminal synaptic targeting elements for postsynaptic density proteins ProSAP1/Shank2 and ProSAP2/Shank3. J. Neurochem. *92*, 519–524.

Brakeman, P.R., Lanahan, A.A., O'Brien, R., Roche, K., Barnes, C.A., Huganir, R.L., and Worley, P.F. (1997). Homer: a protein that selectively binds metabotropic glutamate receptors. Nature *386*, 284–288.

Cheng, D., Hoogenraad, C.C., Rush, J., Ramm, E., Schlager, M.A., Duong, D.M., Xu, P., Wijayawardana, S.R., Hanfelt, J., Nakagawa, T., et al. (2006). Relative and absolute quantification of postsynaptic density proteome isolated from rat forebrain and cerebellum. Mol. Cell. Proteomics *5*, 1158–1170.

Ehlers, M.D. (2003). Activity level controls postsynaptic composition and signaling via the ubiquitin-proteasome system. Nat. Neurosci. *6*, 231–242.

Fritschy, J.M., Harvey, R.J., and Schwarz, G. (2008). Gephyrin: where do we stand, where do we go? Trends Neurosci. *31*, 257–264.

Hayashi, M.K., Ames, H.M., and Hayashi, Y. (2006). Tetrameric hub structure of postsynaptic scaffolding protein homer. J. Neurosci. *26*, 8492–8501.

Hayashi, Y., and Majewska, A.K. (2005). Dendritic spine geometry: functional implication and regulation. Neuron *46*, 529–532.

Im, Y.J., Lee, J.H., Park, S.H., Park, S.J., Rho, S.H., Kang, G.B., Kim, E., and Eom, S.H. (2003). Crystal structure of the Shank PDZ-ligand complex reveals a class I PDZ interaction and a novel PDZ-PDZ dimerization. J. Biol. Chem. *278*, 48099–48104.

Irie, K., Nakatsu, T., Mitsuoka, K., Miyazawa, A., Sobue, K., Hiroaki, Y., Doi, T., Fujiyoshi, Y., and Kato, H. (2002). Crystal structure of the Homer 1 family conserved region reveals the interaction between the EVH1 domain and own proline-rich motif. J. Mol. Biol. *318*, 1117–1126.

Kunishima, N., Shimada, Y., Tsuji, Y., Sato, T., Yamamoto, M., Kumasaka, T., Nakanishi, S., Jingami, H., and Morikawa, K. (2000). Structural basis of glutamate recognition by a dimeric metabotropic glutamate receptor. Nature *407*, 971–977.

Lee, S.H., Choi, J.H., Lee, N., Lee, H.R., Kim, J.I., Yu, N.K., Choi, S.L., Kim, H., and Kaang, B.K. (2008). Synaptic protein degradation underlies destabilization of retrieved fear memory. Science *319*, 1253–1256.

Lim, S., Naisbitt, S., Yoon, J., Hwang, J.I., Suh, P.G., Sheng, M., and Kim, E. (1999). Characterization of the Shank family of synaptic proteins. Multiple genes, alternative splicing, and differential expression in brain and development. J. Biol. Chem. *274*, 29510–29518.

Lu, J., Helton, T.D., Blanpied, T.A., Racz, B., Newpher, T.M., Weinberg, R.J., and Ehlers, M.D. (2007). Postsynaptic positioning of endocytic zones and AMPA receptor cycling by physical coupling of dynamin-3 to Homer. Neuron *55*, 874–889.

Mears, J.A., Ray, P., and Hinshaw, J.E. (2007). A corkscrew model for dynamin constriction. Structure *15*, 1190–1202.

Minakami, R., Kato, A., and Sugiyama, H. (2000). Interaction of Vesl-1L/Homer 1c with syntaxin 13. Biochem. Biophys. Res. Commun. *272*, 466–471.

Mio, K., Ogura, T., Kiyonaka, S., Hiroaki, Y., Tanimura, Y., Fujiyoshi, Y., Mori, Y., and Sato, C. (2007). The TRPC3 channel has a large internal chamber surrounded by signal sensing antennas. J. Mol. Biol. *367*, 373–383.

Mizutani, A., Kuroda, Y., Futatsugi, A., Furuichi, T., and Mikoshiba, K. (2008). Phosphorylation of Homer3 by calcium/calmodulin-dependent kinase II regulates a coupling state of its target molecules in Purkinje cells. J. Neurosci. *28*, 5369–5382.

Naisbitt, S., Kim, E., Tu, J.C., Xiao, B., Sala, C., Valtschanoff, J., Weinberg, R.J., Worley, P.F., and Sheng, M. (1999). Shank, a novel family of postsynaptic density proteins that binds to the NMDA receptor/PSD-95/GKAP complex and cortactin. Neuron *23*, 569–582.

Okabe, S. (2007). Molecular anatomy of the postsynaptic density. Mol. Cell. Neurosci. *34*, 503–518.

Palczewski, K., Kumasaka, T., Hori, T., Behnke, C.A., Motoshima, H., Fox, B.A., Le Trong, I., Teller, D.C., Okada, T., Stenkamp, R.E., et al. (2000). Crystal structure of rhodopsin: a G protein-coupled receptor. Science *289*, 739–745.

Peng, J., Kim, M.J., Cheng, D., Duong, D.M., Gygi, S.P., and Sheng, M. (2004). Semiquantitative proteomic analysis of rat forebrain postsynaptic density fractions by mass spectrometry. J. Biol. Chem. *279*, 21003–21011.

Petersen, J.D., Chen, X., Vinade, L., Dosemeci, A., Lisman, J.E., and Reese, T.S. (2003). Distribution of postsynaptic density (PSD)-95 and Ca2+/calmodulin-dependent protein kinase II at the PSD. J. Neurosci. *23*, 11270–11278.

Romorini, S., Piccoli, G., Jiang, M., Grossano, P., Tonna, N., Passafaro, M., Zhang, M., and Sala, C. (2004). A functional role of postsynaptic density-95-guanylate kinase-associated protein complex in regulating Shank assembly and stability to synapses. J. Neurosci. *24*, 9391–9404.

Sala, C., Piech, V., Wilson, N.R., Passafaro, M., Liu, G., and Sheng, M. (2001). Regulation of dendritic spine morphology and synaptic function by Shank and Homer. Neuron *31*, 115–130.

Sala, C., Futai, K., Yamamoto, K., Worley, P.F., Hayashi, Y., and Sheng, M. (2003). Inhibition of dendritic spine morphogenesis and synaptic transmission by activity-inducible protein Homer1a. J. Neurosci. *23*, 6327–6337.

Sato, C., Hamada, K., Ogura, T., Miyazawa, A., Iwasaki, K., Hiroaki, Y., Tani, K., Terauchi, A., Fujiyoshi, Y., and Mikoshiba, K. (2004). Inositol 1,4,5-trisphosphate receptor contains multiple cavities and L-shaped ligand-binding domains. J. Mol. Biol. *336*, 155–164.

Sheng, M., and Hoogenraad, C.C. (2007). The postsynaptic architecture of excitatory synapses: a more quantitative view. Annu. Rev. Biochem. *76*, 823–847.

Shiraishi-Yamaguchi, Y., and Furuichi, T. (2007). The Homer family proteins. Genome Biol. *8*, 206.

Spacek, J., and Harris, K.M. (1997). Three-dimensional organization of smooth endoplasmic reticulum in hippocampal CA1 dendrites and dendritic spines of the immature and mature rat. J. Neurosci. *17*, 190–203.

Sugiyama, Y., Kawabata, I., Sobue, K., and Okabe, S. (2005). Determination of absolute protein numbers in single synapses by a GFP-based calibration technique. Nat. Methods *2*, 677–684.

Tu, J.C., Xiao, B., Naisbitt, S., Yuan, J.P., Petralia, R.S., Brakeman, P., Doan, A., Aakalu, V.K., Lanahan, A.A., Sheng, M., et al. (1999). Coupling of mGluR/Homer and PSD-95 complexes by the Shank family of postsynaptic density proteins. Neuron *23*, 583–592.

Worley, P.F., Zeng, W., Huang, G., Kim, J.Y., Shin, D.M., Kim, M.S., Yuan, J.P., Kiselyov, K., and Muallem, S. (2007). Homer proteins in Ca2+ signaling by excitable and non-excitable cells. Cell Calcium *42*, 363–371.

Yuan, J.P., Kiselyov, K., Shin, D.M., Chen, J., Shcheynikov, N., Kang, S.H., Dehoff, M.H., Schwarz, M.K., Seeburg, P.H., Muallem, S., et al. (2003). Homer binds TRPC family channels and is required for gating of TRPC1 by IP3 receptors. Cell *114*, 777–789.